Broadband Plasmonic Bandstop Filters With a Single Rectangular Ring Resonator

Yuhsin Chang and Chyong-Hua Chen

***Abstract*— A broadband plasmonic bandstop filter with a single directly connected rectangular ring resonator is proposed. Inside this resonator, which is constructed using two nonidentical branches, both ring resonance and Mach–Zehnder interference occurred. A broad stopband can be realized by appropriately adjusting the resonant wavelengths of these two interferences. An equivalent circuit model is established to analytically describe the performance of this structure and to systematically target its design parameters to achieve the minimal transmittance in the stopband. An example of the plasmonic bandstop filter with its dimensions of 200 nm × 522 nm and stopband edge wavelengths of 1300 and 1800 nm is numerically demonstrated.**

***Index Terms*— Integrated optics, optical filters, optical resonators.**

I. Introduction

PLASMONIC waveguides have attracted much attention in ultrahigh-density photonic integrated circuits (PICs) owing to their highly lateral mode confinement beyond the diffraction limit [1]. Among several plasmonic waveguides, metal -insulator-metal (MIM) waveguides have the properties of easy fabrication, strong field confinement, and relatively low bending and propagation losses [2]. In addition, the propagation behavior of MIM waveguides in the optical region is similar to that of a parallel-plate transmission line in the microwave domain [3]. Thus, MIM-based plasmonic devices can be characterized or designed by using the transmission line theory instead of the complicated full-wave simulation [4], [5].

Bandstop filters with a bandwidth covering from the O band to the L band are an essential component for the application of coarse wavelength-division multiplexing (CWDM) systems [6]. In literature, two schemes have been proposed to possess the stopband over these wavelength regions. One scheme is the Bragg grating structure, whose photonic bandgap is widened by introducing a material with a higher refractive index in the narrow slot waveguide [7], [8]. The other scheme is the cascaded resonator structure [9]–[11], whose stopband is expanded by serially connecting several resonators with different resonant wavelengths. However, to realize low transmissions with minimal ripples in the stopband, the sizes of these devices were enlarged by increasing either the number of the grating cells or the resonators [12], which is thereby inadequate for the application of ultrahigh-density PICs.

Manuscript received May 11, 2014; revised July 2, 2014; accepted July 21, 2014. Date of publication July 29, 2014; date of current version September 8, 2014.

The authors are with the Department of Photonics and Institute of Electro-Optical Engineering, National Chiao Tung University, Hsinchu 300, Taiwan (e-mail: ysyuhsin.chang@gmail.com; chyong@mail.nctu.edu.tw).

Digital Object Identifier 10.1109/LPT.2014.2343517

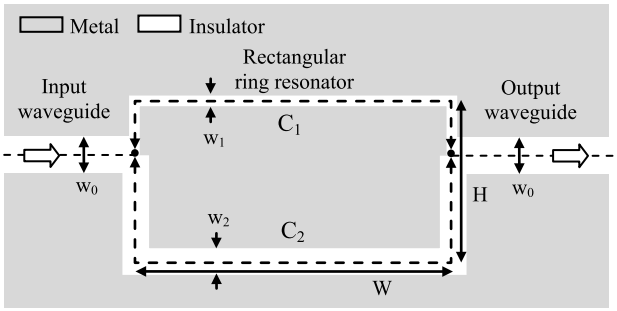

Fig. 1. Schematic diagram of the proposed broadband bandstop filter.

It is known that both ring resonance (RR) and Mach-Zehnder interference (MZI) may occur inside a directly connected plasmonic ring resonator due to the excitation of both the clockwise and the anti-clockwise propagating SP modes there [13], [14]. However, the resonance for the destructive interference of the MZI does not occur in a resonator with two identical branches, giving rise to a Lorentzian-shaped spectral response [13]. Here, we present a nanoplamonic bandstop filter with a flat and broad stopband based on the MIM waveguides achieved by using a directly connected rectangular ring resonator comprised of two non-identical branches, where both RR and MZI occurred. Using the equivalent circuit model based on the transmission line theory, we develop a design procedure to systematically realize a broadband bandstop filter by properly locating the resonant wavelengths of the RR and the MZI. An example of the filter with dimensions of 200 nm × 522 nm and stopband edge wavelengths of 1300 nm and 1800 nm is numerically demonstrated. The calculated results are consistent with the simulated results obtained using the two-dimensional (2D) finite difference time domain (FDTD) method.

II. Analysis of the Broadband Bandstop Filters

A schematic diagram of the proposed broadband bandstop filter is shown in Fig. 1. The input and output waveguides are directly connected to a single rectangular ring resonator. The ring resonator is divided into two branches C_1 and C_2. Both waveguide widths of the input and output waveguides are w_0 to obtain the maximized transmission in the passband. The width and the height of the rectangular ring resonator are W and H, respectively. Let the waveguide width and the length of the branch C_i be w_i and L_i, respectively, for i=1 and i=2. Then, $L_1+L_2 = 2(W+H)$.

Because the input/output waveguide is directly connected to the ring resonator, the wave propagates both clockwise and anti-clockwise in both branches C_1 and C_2 due to the

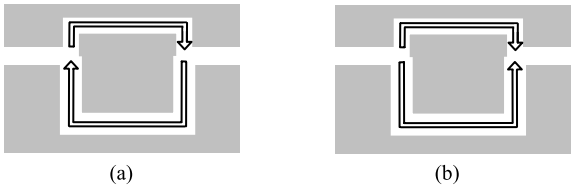

Fig. 2. Schematic diagrams of the wave propagations inside the ring resonator for the interference mechanisms of (a) RR and (b) MZI.

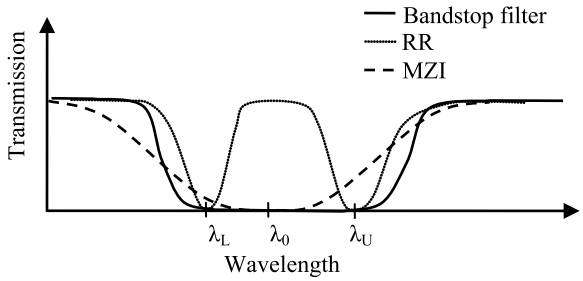

Fig. 3. Schematic of the relative resonant wavelengths of RR and MZI.

impedance mismatch of the T-branch at the intersections. Then, the RR occurs as the wave circulates in the branches C_1 and C_2 either clockwise or anti-clockwise as shown in Fig. 2(a). In contrast, the MZI appears as the wave in the branch C_1 propagates in the opposite direction of that in the branch C_2, as illustrated in Fig. 2(b).

The resonant wavelengths of these two phenomena are different, and we can manipulate these resonant wavelengths to implement a broadband bandstop filter as follows. Suppose a bandstop filter has a notch-shaped transmission spectrum with upper and lower stopband edge wavelengths of λ_U and λ_L, respectively. Because the difference between the adjacent resonant wavelengths of the RR is smaller than that of the MZI, we assign the first- and second-order resonant wavelengths of the RR as λ_U and λ_L, respectively. Subsequently, the wavelength for the destructive interference of the MZI is located between λ_U and λ_L to flatten the transmission in the stopband region. The relative locations of these resonant wavelengths are delineated in Fig. 3. It is known that the transmission in the stopband is minimized only when the completely destructive interferences occur at these resonant wavelengths. Therefore, we use the transmission line theory to analyze the wave behavior inside this structure to accomplish a low transmission at these resonances and then establish a design procedure to achieve a broadband bandstop filter with the given specifications.

An equivalent circuit model based on the transmission line theory is employed to analyze this structure. The characteristic impedances of the input and output waveguides are calculated by $Z_0 = (\beta_0 w_0)/(\omega\varepsilon_0\varepsilon_d)$ [15], where β_0 is the propagation constant of the input/output waveguide, ω is the incident frequency, ε_0 is the permittivity of free space and ε_d is the relative permittivity of the insulator. Then, each segment of the branch C_i is represented by a symmetric T-type equivalent circuit with the impedances of [16]

$$Z_{ia} = iZ_i \tan(\beta_i L_i/2). \quad (1)$$

$$Z_{ib} = -iZ_i/\sin(\beta_i L_i). \quad (2)$$

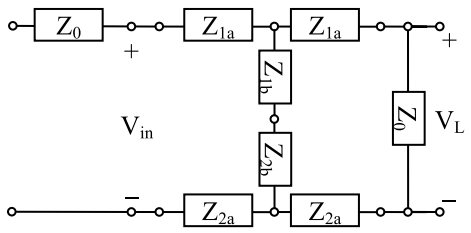

Fig. 4. Equivalent circuit model of the proposed structure.

where $Z_i = (\beta_i w_i)/(\omega\varepsilon_0\varepsilon_d)$ is the characteristic impedance of the branch C_i with the corresponding propagation constant of β_i, for i=1 and i=2.

The equivalent circuit of this proposed structure is illustrated in Fig. 4. The voltage at the input port is $V_{in} = V_0^+ + V_0^-$, where V_0^+ and V_0^- are the complex amplitudes of the incident and reflected voltage waves, respectively. The load voltage at the output port is V_L. Then, the transmission T at the output port is calculated as

$$T = \left|\frac{V_L}{V_0^+}\right|^2 = \left|\frac{2Z_0(Z_{1b}+Z_{2b})}{(Z_0+Z_{1a}+Z_{2a})(Z_0+Z_{1a}+Z_{2a}+2Z_{1b}+2Z_{2b})}\right|^2. \quad (3)$$

From (3), the maximal transmission is 1 without taking the loss of the structure into account. The transmission in the whole spectrum is zero at $Z_0 = 0$ or ∞ or $Z_1 = Z_2 = 0$ or ∞, but these extreme cases are not concerned for a bandstop filter design. Besides, we see that low transmission can be obtained if either $Z_{1b}+Z_{2b}$ is zero, or if Z_{1a} or Z_{2a} approaches infinity. $Z_{1b}+Z_{2b}$ is zero when $Z_1\sin(\beta_2 L_2)+Z_2\sin(\beta_1 L_1)=0$. This formulation shows that the interference of the clockwise and anti-clockwise circulating waves inside the resonator is completely destructive in the output waveguide, where Z_1 and Z_2 are relevant to the transmission coefficients of the two branches in an opened T-branch splitter. Thus, this expression corresponds to the condition of the zero-transmission RR, but the minimal transmission can be obtained as $\mathrm{Re}\{Z_1\sin(\beta_2 L_2)+Z_2\sin(\beta_1 L_1)\}=0$ due to the propagation losses of the SPP modes. In accordance with the aforementioned design concept, the stopband edge wavelengths must satisfy the following conditions, respectively.

$$Re\{\beta_1(\lambda_U)w_1\sin(\beta_2(\lambda_U)L_2)+\beta_2(\lambda_U)w_2\sin(\beta_1(\lambda_U)L_1)\} = 0 \quad (4)$$

$$Re\{\beta_1(\lambda_L)w_1\sin(\beta_2(\lambda_L)L_2)+\beta_2(\lambda_L)w_2\sin(\beta_1(\lambda_L)L_1)\} = 0 \quad (5)$$

On the other hand, Z_{1a} or Z_{2a} is near infinity when $\mathrm{Re}\{\beta_i\}L_i = m\pi$, where m is an odd integer for i=1 and i=2. However, when examining (3), we find that the transmission is approximately zero only at $\mathrm{Re}\{\beta_1 L_1 - \beta_2 L_2\}=(2m+1)\pi$ for an arbitrary integer m. That is, the minimal transmission is obtained as the phase shift difference of the two branches C_1 and C_2 is an odd multiple of π, corresponding to the condition for the completely destructive interference of the MZI.

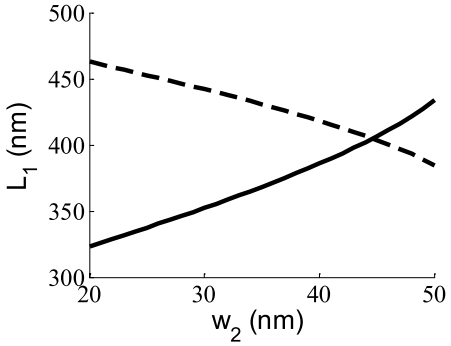

Fig. 5. Graphical solution sets $\{w_2, L_1\}$ for (8) (solid curve) and (9) (dashed curve) with $w_1 = 20$ nm, $\lambda_L = 1300$ nm and $\lambda_U = 1800$ nm.

Then, the resonant wavelength of the MZI λ_0 can be chosen to comply with the conditions of

$$Re\{\beta_1(\lambda_0)\}L_1 = \pi \quad (6)$$

$$Re\{\beta_2(\lambda_0)\}L_2 = 2\pi \quad (7)$$

Then, $\mathrm{Re}\{\beta_1(\lambda_U)\}L_1 < \pi$ because λ_U is the first-order resonant wavelengths of the RR, respectively.

As shown in (4) to (7), the properties of the low transmission band are independent of w_0, and roughly depend on the ratio of w_1 to w_2. In addition, (6) and (7) indicate that the phase shift of the branch C_2 is approximately twice that of the branch C_1. Then, (4) and (5) can be rewritten roughly as

$$Re\{2\beta_1(\lambda_U)w_1\cos(\beta_1(\lambda_U)L_1) + \beta_2(\lambda_U)w_2\} = 0 \quad (8)$$

$$Re\{2\beta_1(\lambda_L)w_1\cos(\beta_1(\lambda_L)L_1) + \beta_2(\lambda_L)w_2\} = 0 \quad (9)$$

These two equations represent the relationship between the length of the branch C_1 and the width of the branch C_2 when w_1 is determined. Accordingly, we can choose a certain w_1 and can numerically obtain L_1 and w_2 by solving (8) and (9). Then, the resonant wavelength of the MZI λ_0 and L_2 are attained by solving (6) and (7), respectively. In the next section, we exhibit examples of the bandstop filters with the given specifications based on these procedures.

III. Design Examples and Discussion

For proof-of-concept, the dielectric and metallic materials of the MIM waveguides are air and silver, respectively. The permittivity of the silver ε_m is described by the Drude-Lorentz model [17]. The dispersion relation between the propagation constant β and the width of the MIM waveguide can be found in reference [13] in detail.

Supposed that the concerned stopband filter has stopband edge wavelengths of $\lambda_L = 1300$ nm and of $\lambda_U = 1800$ nm. First, we arbitrarily choose $w_0 = 50$ nm and set $w_1 = 20$ nm. Because $\mathrm{Re}\{\beta_1(\lambda_U)\}L_1 < \pi$, L_1 has to be less than 484.8 nm. Additionally, w_2 has to be roughly smaller than 50 nm to have a valid solution. Figure 5 illustrates the graphical solution sets of $\{w_2, L_1\}$for (8) and (9). Two curves intersect at L_1 equal to 405 nm and at w_2 equal to 44 nm. Then, the corresponding λ_0 is 1510 nm, and L_2 is 1038 nm by solving (6) and (7), respectively.

To avoid the coupling between two adjacent waveguides, the resonator width W is chosen as 200 nm, and then the corresponding height H is 522 nm, i.e., the dimensions of the rectangular waveguide is 200 nm × 522 nm. The transmission spectra for the aforementioned resonator are calculated by (3) and are simulated by a 2D FDTD simulator (Fullwave, RSOFT Design Inc.) as shown in Fig. 6. A low transmission of less than 0.0013 is obtained over the wavelength range of 1300 nm and 1800 nm. A maximum transmission of approximately 0.76 is obtained at the resonant wavelengths for the completely constructive interference of the MZI, i.e., $\mathrm{Re}\{\beta_1 L_1 - \beta_2 L_2\} = 2m\pi$, where m is an integer. The absorption of the whole structure is approximately 1.1 dB and is primarily attributed to the propagation loss inside the ring resonator. In comparison with the calculated data, the simulated FDTD results are in close agreement, except that the whole spectrum shifts to a shorter wavelength by approximately 50 nm.

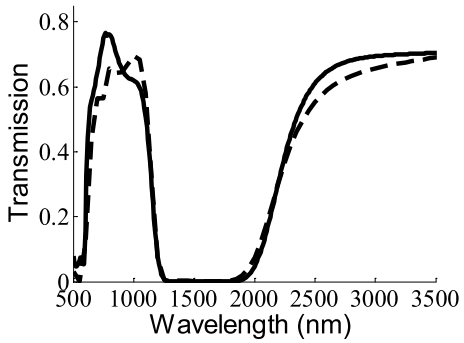

Fig. 6. Transmission spectra of the proposed structure calculated by the equivalent circuit model (solid curve) and the FDTD method (dashed curve) with $w_1 = 20$ nm, $w_2 = 44$ nm, $L_1 = 405$ nm, $L_2 = 1038$ nm, $W = 200$ nm and $H = 522$ nm.

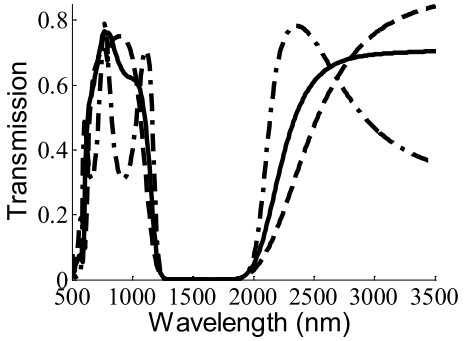

Fig. 7. Variation of w_1 on the transmission spectrum. Transmission spectra of three designs with $w_0 = 50$ nm: $w_1 = 10$ nm, $w_2 = 24$ nm, $L_1 = 308$ nm and $L_2 = 864$ nm (dashed curve); $w_1 = 20$ nm, $w_2 = 44$ nm, $L_1 = 405$ nm and $L_2 = 1038$ nm (solid curve); and $w_1 = 50$ nm, $w_2 = 100$ nm, $L_1 = 536$ nm and $L_2 = 1236$ nm (dashed-dotted curve).

Figure 7 shows the transmission spectra for different values of w_1. The aforementioned design procedure is applied to obtain the design parameters of the bandstop filters with the same specifications for a different w_1. We see that the transmission over the wavelength range of 1300 nm and 1800 nm is less than 0.002 in all designs. In addition, the transition band becomes sharper as w_1 increases as a result of increasing L_1. From (3), the local minimal transmission in the passband is roughly $(1+|Z_1/Z_0|^2)^{-1}$ at the wavelength for $\mathrm{Re}\{\beta_1\}L_1 = (2m+1)\pi/2$, where m is an integer. This result demonstrated that the passband ripple is pertinent to the ratio of w_1 to w_0. Then, the concomitant passband ripples increase with the increment of w_1 as observed in Fig. 7.

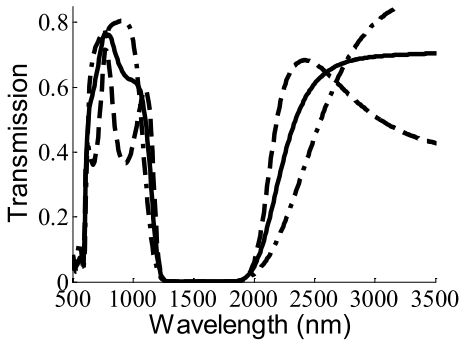

Fig. 8. Transmission spectra with $w_0 = 25$ nm (dashed curve), 50 nm (solid curve) and 100 nm (dashed-dotted curve). Here, $w_1 = 20$ nm, $w_2 = 44$ nm, $L_1 = 405$ nm and $L_2 = 1038$ nm.

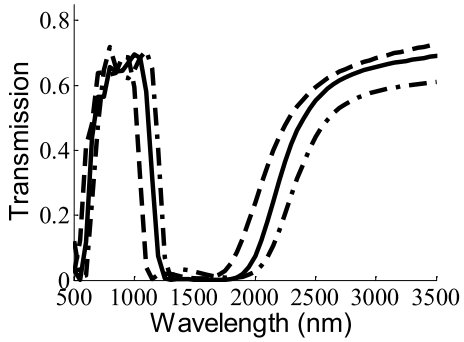

Fig. 9. The transmission spectra with different ratios η:$\eta = 0.9$ (dashed curve), $\eta = 1$ (solided curve) and $\eta = 1.1$ (dashed-dotted curve).

The effect of w_0 on the transmission spectra of the ring resonator with $w_1 = 20$ nm, $w_2 = 44$ nm, $L_1 = 405$ nm and $L_2 = 1038$ nm is shown in Fig. 8. Similar transmission responses in the stopband are acquired in all designs, revealing that w_0 slightly affects the characteristics of the stopband. However, the transition band becomes wider, the maximal transmission is larger and the concomitant passband ripples decreases as w_0 is widened.

The effect of fabrication imperfections on the transmission spectrum of the aforementioned device is illustrated in Fig. 9. Here, all the geometrical parameters (i.e., W, L, w_1, w_2, L_1 and L_2) are varied by a ratio η. As shown in Fig. 9, the transmission spectrum shifts to a longer wavelength as η increases. Small ripples in the stopband are obtained due to the incompletely destructive interference of the MZI.

IV. Conclusion

A broadband plasmonic bandstop filter with a single directly connected rectangular ring resonator based on MIM waveguides is analytically investigated and numerically demonstrated. Because of the direct connection between the input/output waveguides and the resonator, the waves are allowed to propagate in both the clockwise and anticlockwise directions inside the resonator, giving rise to both RR and MZI. To realize a broad bandwidth for the bandstop filter, we maneuver the first and second resonant wavelengths of the RR to be the upper and lower stopband edge wavelengths, respectively, and the resonant wavelength for the completely destructive interference of the MZI is located between these two wavelengths.

Next, to obtain a low transmission in the stopband, we analytically describe the performance of this rectangular ring resonator by using the equivalent circuit model based on the transmission line theory and then develop a systematic design procedure to carry out the geometrical parameters of a plasmonic bandstop filter with the given specifications. An example of a rectangular ring resonator with its dimensions of 200 nm $\times$ 522 nm is numerically demonstrated to achieve a bandstop filter with stopband edge wavelengths of 1300 nm and 1800 nm. The performance of the design is also confirmed by using the 2D FDTD method. A higher maximal transmission and smaller passband ripples can be obtained by decreasing the ratio of w_1 to w_0.

References

[1] E. Ozbay, "Plasmonics: Merging photonics and electronics at nanoscale dimensions," *Science*, vol. 311, no. 5758, pp. 189–193, Jan. 2006.

[2] G. Veronis and S. Fan, "Bends and splitters in metal-dielectric-metal subwavelength plasmonic waveguides," *Appl. Phys. Lett.*, vol. 87, no. 13, pp. 131102-1–131102-3, Sep. 2005.

[3] T. Takano and J. Hamasaki, "Propagating modes of a metal-clad-dielectric-slab waveguide for integrated optics," *IEEE J. Quantum Electron.*, vol. QE-8, no. 2, pp. 206–212, Feb. 1972.

[4] Y. Matsuzaki, T. Okamoto, M. Haraguchi, M. Fukui, and M. Nakagaki, "Characteristics of gap plasmon waveguide with stub structures," *Opt. Exp.*, vol. 16, no. 21, pp. 16314–16325, Oct. 2008.

[5] M. Rezaei *et al.*, "A distributed circuit model for side-coupled nanoplasmonic structures with metal–insulator–metal arrangement," *IEEE J. Sel. Topics Quantum Electron.*, vol. 18, no. 6, pp. 1692–1699, Nov./Dec. 2012.

[6] *Spectral Grids for WDM Applications: CWDM Wavelength Grid*, document ITU-T G.694.2, Geneva, Switzerland, 2003.

[7] J.-Q. Liu *et al.*, "A wide bandgap plasmonic Bragg reflector," *Opt. Exp.*, vol. 16, no. 7, pp. 4888–4894, Mar. 2008.

[8] Y. Liu, Y. Liu, and J. Kim, "Characteristics of plasmonic Bragg reflectors with insulator width modulated in sawtooth profiles," *Opt. Exp.*, vol. 18, no. 11, pp. 11589–11598, May 2010.

[9] J. Liu, G. Fang, H. Zhao, Y. Zhang, and S. Liu, "Surface plasmon reflector based on serial stub structure," *Opt. Exp.*, vol. 17, no. 22, pp. 20134–20139, Oct. 2009.

[10] P.-H. Lee and Y.-C. Lan, "Plasmonic waveguide filters based on tunneling and cavity effects," *Plasmonics*, vol. 5, no. 4, pp. 417–422, Dec. 2010.

[11] Z. H. Zhu, Z. H. Han, and S. I. Bozhevolnyi, "Wide-bandwidth polarization-independent optical band-stop filter based on plasmonic nanoantennas," *Appl. Phys. A*, vol. 110, no. 1, pp. 71–75, 2013.

[12] C. Xu, H. Ting, R. Chen, Y. Ping, J. Yang, and X. Jiang, "Transmission characteristics of a plasmonic Bragg reflector based on a metal-embedded slot structure," *J. Opt.*, vol. 15, no. 10, p. 105005, 2013.

[13] V. F. Nezhad, S. Abaslou, and M. S. Abrishamian, "Plasmonic band-stop filter with asymmetric rectangular ring for WDM networks," *J. Opt.*, vol. 15, no. 5, p. 055007, 2013.

[14] B. Wang and G. P. Wang, "Surface plasmon polariton propagation in nanoscale metal gap waveguides," *Opt. Lett.*, vol. 29, no. 17, pp. 1992–1994, Sep. 2004.

[15] H. Nejati and A. Beirami, "Theoretical analysis of the characteristic impedance in metal-insulator-metal plasmonic transmission lines," *Opt. Lett.*, vol. 37, no. 6, pp. 1050–1052, Mar. 2012.

[16] K. Chang and L. H. Hsieh, "Analysis and modeling of ring resonators," in *Microwave Ring Circuits and Related Structures*, 2nd ed. New York, NY, USA: Wiley, 2004, p. 24.

[17] P. B. Johnson and R. W. Christy, "Optical constants of the noble metals," *Phys. Rev. B*, vol. 6, no. 12, pp. 4370–4379, Dec. 1971.